A Simple Technique for Open-Stopband Suppression in Periodic Leaky-Wave Antennas Using Two Nonidentical Elements Per Unit Cell

Juhua Liu, *Member, IEEE*, Wenlong Zhou, and Yunliang Long, *Senior Member, IEEE*

***Abstract*— A simple technique is presented for the complete suppression of the open stopband in periodic leaky-wave antennas using two similar but nonidentical elements per unit cell. With the technique, one needs only to optimize the distance between the two elements and the dimension of the second element, starting with a quarter of the period and the dimension of the first element. With the simple design procedure, the technique is practical and effective for the open-stopband suppression for various periodic leaky-wave antennas. Two periodic leaky-wave antennas with the technique are demonstrated. The first one is a new developed substrate-integrated waveguide antenna with two nonidentical transverse slots per unit cell. The antenna has a wide scanning range from the backward endfire to the forward direction and does not suffer from blind scanning points at endfires (if it is placed on an infinite ground plane). The antenna is theoretically investigated. The simulation and measured results are consistent with the theoretical results. The second one is a microstrip combline leaky-wave antenna, in which each unit cell contains two nonidentical open-ended stubs. The two examples validate that the technique proposed in this paper can completely eliminate the open stopband in periodic leaky-wave antennas.**

***Index Terms*— Combline leaky-wave antenna, open stopband, periodic leaky-wave antenna, substrate-integrated waveguide (SIW), two nonidentical elements.**

I. Introduction

THE 1-D leaky-wave antennas are attractive due to the advantages of simple structure, high gain, and beam-scanning capability. A myriad of leaky-wave antennas have been proposed based on various technologies, e.g., waveguide [1]–[3], dielectric image line [4], microstrip line [5]–[15], substrate-integrated waveguide (SIW) [16]–[28], and groundless spoof plasmons structure [29].

The 1-D leaky-wave antennas can be divided into three categories, depending on whether the structure is uniform, quasi-uniform, or periodic [30]. The radiation of the uniform or conventional quasi-uniform leaky-wave antennas is from the fundamental space harmonic (fast wave), so the main beam can only be scanned in the first forward quadrant space. An exception is the kind of quasi-uniform leaky-wave antennas based on metamaterials, e.g., the microstrip composite right-/left-handed (CRLH) (quasi-uniform) leaky-wave antennas [8], which have the beam scanned in the backward and the forward quadrant spaces. In these two types of leaky-wave antennas, the radiation angle of the main beam $\theta'_{\max}$ [measured from the normal direction, i.e., the y-axis as shown in Fig. 1(a)] is determined by $\sin\theta'_{\max} = \beta/k_0$, where β is the phase constant of the fundamental space harmonic and k_0 is the free-space wavenumber. The periodic leaky-wave antenna, in which the fundamental space harmonic is a slow wave, usually radiates from the fast $n = -1$ space harmonic [30], and can also have the main beam scanned in the backward and the forward quadrant spaces. In the periodic leaky-wave antenna, the radiation angle is determined by

$$\sin\theta'_{\max} = \beta_{-1}/k_0 \tag{1}$$

where β_{-1} is the phase constant of the $n = -1$ space harmonic. The phase constant of the nth space harmonic is calculated by

$$\beta_n = \beta + \frac{2n\pi}{p} \tag{2}$$

where p is the period of the structure. Though the CRLH leaky-wave antenna and the periodic leaky-wave antenna can have the beam in the backward or the forward direction, they usually suffer from an open stopband when the main beam is scanned through broadside. In the open-stopband region, a high reflection coefficient is encountered and the radiated power drops substantially.

In a CRLH leaky-wave antenna, the open stopband can be eliminated using the so-called balanced transmission line [8]. With the elimination of the open stopband, the antenna can have its main beam scanned seamlessly through broadside.

For periodic leaky-wave antennas, several techniques were proposed for suppressing the open stopband. A pair of identical elements spaced approximately a quarter of the period for each unit cell can be used for mitigating the open-stopband effects [4]–[6]. The technique has the advantage of simplicity, and can be applied to various periodic structures, e.g., dielectric image line structure [4] and microstrip periodic

Manuscript received September 17, 2017; revised December 20, 2017; accepted January 10, 2018. Date of publication March 26, 2018; date of current version May 31, 2018. This work was supported in part by the Natural Science Foundation of China under Grant 61771497, Grant 61401522, Grant 41376041, and Grant 61172026, and in part by the NSF of Guangdong Province under Grant 2015A030312010. *(Corresponding author: Juhua Liu.)*

The authors are with the Department of Electronics and Communication Engineering, Sun Yat-sen University, Guangzhou 510006, China (e-mail: liujh33@mail.sysu.edu.cn).

Color versions of one or more of the figures in this paper are available online at http://ieeexplore.ieee.org.

Digital Object Identifier 10.1109/TAP.2018.2819701

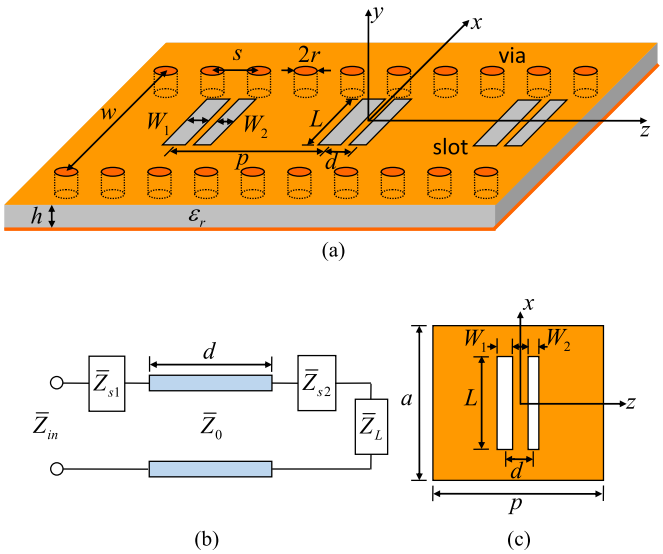

Fig. 1. (a) Geometry of the proposed SIW periodic leaky-wave structure. (b) Approximate equivalent circuit for one cell of the periodic structure. (c) Top view of one cell in the equivalent rectangular waveguide.

structure [5], [6]. However, usually the open stopband cannot be completely suppressed using the technique.

In [9], a quarter-wave transformer or a matching stub was introduced to eliminate the open stopband in a printed periodic leaky-wave antenna. A prototype of a combline leaky-wave antenna was fabricated and measured [10], to validate the technique presented in [9]. The technique can be conveniently used for a printed periodic structure, but is not simple enough for a rectangular waveguide or an SIW structure.

In [11]–[14], more general studies of the characteristics of the open stopband were reported with respect to the transverse asymmetry, longitudinal asymmetry, or double asymmetry in a structure. In [12], it was demonstrated that a periodic leaky-wave antenna with its unit cell asymmetry with respect to the transverse axis can be leveraged for suppressing the open stopband in a periodic leaky-wave antenna. However, it is complicated to design a periodic structure with the open stopband suppressed using the method [12]. In the analysis in [12], the problem is addressed via an equivalent circuit composed of a series resonator, a shunt resonator, and the transformation ratio for modeling asymmetry. To design an open-stopband suppressed structure using the method [12], one should first balance the series and shunt frequencies for frequency balancing, and second adjust the degree of asymmetry for quality factor balancing. For frequency balancing the series and shunt frequencies, the LCRG parameters in the circuit must be extracted beforehand [12], where L and C are the reactance and susceptance slope parameters, R is the series resistance and G is the shunt conductance.

Besides these techniques, some special leaky-wave structures with the open stopband suppressed have also been reported. In [26], an SIW leaky-wave antenna with periodic longitudinal slots was reported, which had a high gain and had its open stopband eliminated. However, it is not possible for the antenna with longitudinal slots to radiate at endfires even when it is placed on an infinite ground plane, since the radiation of each slot has nulls at endfires. In [15], a microstrip periodic leaky-wave antenna with circular polarization and wide scanning range was developed. In [29], a single-layer spoof-plasmon-mode leaky-wave antenna was developed, which had wide bandwidth and consistent gain.

Liu *et al.* [21] proposed an SIW quasi-uniform leaky-wave antenna with transverse slots. The antenna has a good scanning capability to forward endfire, since the radiation pattern of each slot does not vanish at endfires, and the structure supports two slow-wave (surface wave and proper waveguide) modes in addition to a fast-wave (leaky-wave) mode. The experiment in [25] validated that an SIW leaky-wave antenna with transverse slots on the top and bottom broad walls could provide an exact endfire beam. However, this type of SIW quasi-uniform antenna is a quasi-uniform leaky-wave antenna [30], so it can only scan in the forward quadrant space.

In this paper, we propose a simple technique for the complete suppression of the open stopband in periodic leaky-wave antennas using two similar but nonidentical elements for each unit cell. Without estimating the series and shunt resonances for frequency balancing, the technique is much simpler than that in [12]. In the design procedure with the proposed technique, one needs only to optimize the distance between the two elements and the dimension of the second element, starting with a quarter of the period and the dimension of the first element. Compared with [9], the technique is expected to be applied to various leaky-wave antennas besides printed leaky-wave antennas.

Two periodic leaky-wave antennas with the open stopband suppressed are demonstrated to validate the effectiveness of the technique. The first one is a new developed SIW antenna with two nonidentical transverse slots per unit cell. The antenna has a high gain, a wide scanning range from the backward endfire to the forward direction, and does not suffer from blind scanning points at endfires (if it is placed on an infinite ground plane). The antenna is theoretically investigated. The simulation and measured results are consistent with the theoretical results. The second one is a combline leaky-wave antenna, in which a unit cell contains two nonidentical open-ended stubs. The two examples validate that the technique proposed in this paper can completely suppress the open stopband in periodic leaky-wave antennas.

II. Theoretical Methods for the SIW Periodic Structure With Two Slots Per Unit Cell

A. Antenna Geometry

The geometry of the developed SIW leaky-wave antenna is shown in Fig. 1(a). The SIW is fabricated on a substrate with a relative permittivity ε_r and a thickness h. Two lines of conductive vias with a pacing w are adopted to short the top and bottom conductors, to construct a wave-guided structure. In each line, the radius of the vias is r, and the distance between two adjacent vias is s.

A periodic set of two similar but nonidentical transverse slots is placed on the top broad wall of the SIW. The period p of the slots is comparable to the guided wavelength of the SIW, which is different from that in [21] where the period p is much

smaller than the wavelength. Therefore, the radiation in this leaky-wave antenna occurs from the $n = -1$ space harmonic but not the fundamental space harmonic [21]. If the antenna unit cell has only one slot, an open stopband occurs, as will be shown in Section III-A. With a similar but nonidentical slot added to each unit cell, the open stopband can be suppressed, as will be shown in Section III-C. As shown in Fig. 1(a), the second slot has a different size $L \times W_2$ and is placed at a distance d from the first slot of $L \times W_1$. (Actually, the second slot is only required to be not identical, but does not have to share the same length or the same width of the first slot.) Here, in order to have an easy calculation using the integral method given in Section II-C, we let the second slot have the same length L but a different width W_2 from the first slot.

B. Approximate Equivalent Circuits

Assume that the Bloch impedance Z_B of the periodic structure [Fig. 1(a)] is very close to the characteristic impedance Z_0 of the unperturbed transmission line (SIW). Then, an equivalent circuit is introduced to approximate the unit cell of the periodic structure that contains two elements (slots) in one period. The approximate circuit is shown in Fig. 1(b), where Z_{s1} and Z_{s2} represent the impedances of the first and the second elements and Z_L represents the load impedance. The impedances are normalized to the characteristic impedance Z_0 of the unperturbed transmission line.

The input impedance of the circuit is

$$\bar{Z}_{\text{in}} = \bar{Z}_{s1} + \frac{(\bar{Z}_L + \bar{Z}_{s2}) + j\bar{Z}_0 \tan \beta d}{\bar{Z}_0 + (\bar{Z}_L + \bar{Z}_{s2}) j \tan \beta d} \tag{3}$$

where β is the phase constant of the transmission line. In the circuit, it is assumed that the line is lossless with a zero attenuation constant.

Since it is assumed that the load impedance is very close to the characteristic impedance of the unperturbed line, we can set

$$\bar{Z}_L \approx \bar{Z}_0 = 1. \tag{4}$$

We can also make an approximation that the impedance of the first element is imaginary or

$$\bar{Z}_{s1} \approx -j\bar{X}. \tag{5}$$

When the distance between the first and the second elements is a quarter wavelength in the transmission line ($\beta d = \pi/2$) and $\bar{Z}_{s2} = \bar{Z}_{s1}$, the input impedance of the cell becomes

$$\bar{Z}_{\text{in}} \approx -j\bar{X} + \frac{1 + j\bar{X}}{1 + \bar{X}^2}. \tag{6}$$

When the impedance of the first element is very small compared with the characteristic impedance of the transmission line or

$$\bar{X} \ll 1 \tag{7}$$

the term $\bar{X}^2$ in (6) can be neglected and the normalized input impedance can be approximated by

$$\bar{Z}_{\text{in}} \approx -j\bar{X} + 1 + j\bar{X} = 1. \tag{8}$$

Then the circuit is matched, and the open stopband is removed accordingly.

When the main beam is in the broadside direction and the radiation is from the $n = -1$ space harmonic, it is implied from (1) that $\beta_{-1} = 0$. With respect to (2), $p = 2\pi/\beta$. Since a condition of $\beta d = \pi/2$ is made in the calculation for (6), we get

$$d = p/4. \tag{9}$$

Hence, in this approximate analysis, it requires that the distance between the two elements is a quarter of the period.

Note that an assumption of $Z_B \approx Z_0$ is made and approximations are also made in (4), (5), and (7). When the impedances of the elements are not of a very small imaginary value or are of a complex value, (8) will not be true and the circuit is not exactly matched. In practical, the impedances of the radiating elements are with a complex value for a leaky-wave structure. Hence, the adoption of two identical elements (exact Z_{s1} and Z_{s2} in the circuit) can usually mitigate but cannot completely suppress the open stopband, as pointed out in [9]. Even with an optimization of the distance (which may not be a quarter guided wavelength any more) between the two identical elements, the open stopband cannot be completely suppressed, since a deep minimum in the attenuation constant occurs [9].

The adoption of two nonidentical elements for the antenna unit cell, on the other hand, can possibly suppress the open stopband, even when the impedances of the radiating elements are with a complex value and the Bloch impedance is not exactly the same as the characteristic impedance of the unperturbed transmission line. However, it is difficult to find an optimal set of parameters for the structure with the open stopband suppressed through matching a simple equivalent circuit, since a more accurate equivalent circuit must be used and all the impedances (including the lumped impedances of the radiating elements) in the equivalent circuit are required to be calculated preliminary. The accurate calculation for the lumped elements is not practical for many periodic structures, e.g., the SIW periodic structure shown in Fig. 1(a).

Alternately, we can find the optimized parameters with which the open stopband is suppressed, through the calculation of the propagation wavenumber $k_z = \beta - j\alpha$ (where β is the phase constant and α is the attenuation constant) using numerical methods (e.g., the integral equation method or HFSS). As previously pointed out in [9], the suppression of the open stopband can be casted in terms of a linear curve of the normalized phase constant of the radiating space harmonic and a flat curve of the normalized attenuation constant, against the frequency around broadside. In addition, the phase constants can be used for determining the radiation direction by (1). Hence, we will next focus on the calculation of the propagation wavenumber.

C. Integral Equation Method

In order to have an accurate modal analysis of the presented SIW periodic structure with two nonidentical slots per unit cell, we employ an integral equation method. Without approximating the transverse slots as lumped elements, the method

is certainly more accurate than that using an equivalent circuit. Compared with a full-wave numerical commercial software (i.e., HFSS), the method can distinguish the modes in the structure by solving an eigenvalue problem, and the calculation is more efficient.

We consider the presented SIW leaky-wave structure [Fig. 1(a)] as an equivalent rectangular waveguide leaky-wave structure [Fig. 1(c)]. The rectangular waveguide has an equivalent width a, which can be calculated by [31]. The other parameters of the rectangular waveguide leaky-wave structure are the same as those in the SIW leaky-wave structure. The tangential electric fields at the aperture in one cell are assumed

$$E_z(x,0,z) = A_1 E_{z1}(x,0,z) + A_2 E_{z2}(x,0,z) \tag{10}$$

where

$$E_{z1}(x,0,z) = \cos\left(\frac{\pi}{L}x\right), |x| \le \frac{L}{2}, \left|z + \frac{d}{2}\right| \le \frac{W_1}{2} \tag{11}$$

and

$$E_{z2}(x,0,z) = \cos\left(\frac{\pi}{L}x\right), |x| \le \frac{L}{2}, \left|z - \frac{d}{2}\right| \le \frac{W_2}{2}. \tag{12}$$

Using the integral equation method [2], a matrix form equation can be obtained

$$\begin{bmatrix} Y_{11} & Y_{12} \\ Y_{21} & Y_{22} \end{bmatrix} \begin{bmatrix} A_1 \\ A_2 \end{bmatrix} = \begin{bmatrix} 0 \\ 0 \end{bmatrix}. \tag{13}$$

The system has nontrivial solution for the propagation wavenumber k_z of the wave-guided structure, given that the determinant of the matrix in (13) vanishes or

$$\det\ [Y_{ij}] = 0 \tag{14}$$

where Y_{ij} represents an element in (13). The element Y_{ij} in (14) can be calculated by

$$Y_{ij} = \sum_{n=-\infty}^{\infty} \Phi_{ij}\, \mathrm{sinc}\left(\frac{k_{zn}W_i}{2}\right) \mathrm{sinc}\left(\frac{k_{zn}W_j}{2}\right) \cdot \left\{ \sum_{m=1,3,5,\ldots}^{\infty} \left[k_1^2 - \left(\frac{m\pi}{a}\right)^2\right] \frac{\cos^2\left(\frac{m\pi L}{2a}\right)}{\left(1 - \frac{m^2L^2}{a^2}\right)^2} \frac{\cot\left(k_{ymn1}h\right)}{k_{ymn1}h} + j\frac{\pi^2}{16}\frac{\mu_r a}{L^2 h} I_n \right\} \tag{15}$$

where $\Phi_{11} = \Phi_{22} = 1$, $\Phi_{12} = e^{jk_{zn}d}$, $\Phi_{21} = e^{-jk_{zn}d}$, and I_n is calculated by

$$I_n = \int_0^{\pi} \left[\left(k_0^2\frac{L^2}{\pi^2} - 1\right)(\pi - r)\cos(r) + \left(k_0^2\frac{L^2}{\pi^2} + 1\right)\sin(r)\right] H_0^{(2)}\left(\frac{k_{\rho n}Lr}{\pi}\right) dr \tag{16}$$

and

$$k_{\rho n} = \sqrt{k_0^2 - k_{zn}^2} \tag{17}$$

$$k_{ymn1} = \sqrt{k_1^2 - (m\pi/a)^2 - k_{zn}^2} \tag{18}$$

$$k_1 = k_0\sqrt{\varepsilon_r(1 - j\tan\delta)} \tag{19}$$

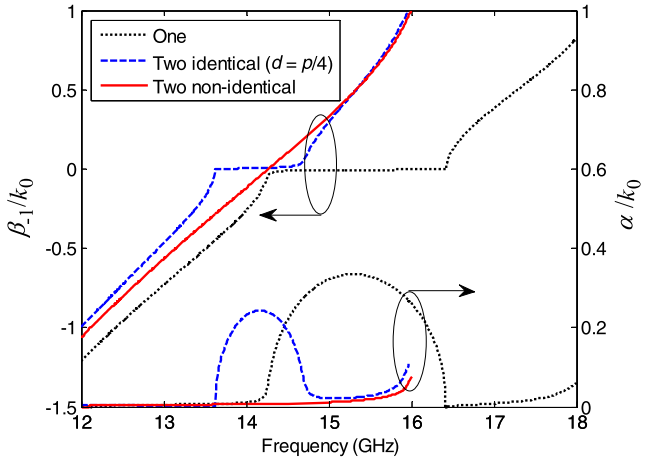

Fig. 2. Theoretical results for the propagation wavenumbers of the rectangular waveguide periodic leaky-wave structures with one slot in each cell, two identical slots in each cell, and two nonidentical slots in each cell. The parameters for the structure with two nonidentical slots are given in the second column in Table I. The other two structures have the same dimensions as the structure with two nonidentical slots in each cell. The slots in the structure with one slot in each cell and in the structure with two identical slots in each cell have the same size as the first slot in the structure with two nonidentical slots in each cell.

and $H_0^{(2)}$is the Hankel function, k_0 is the wavenumber in free space, and ε_r, μ_r, and $\tan\delta$ represent the relative permittivity, relative permeability, and loss tangent of the substrate in the waveguide.

III. Dispersion Curves for the SIW Periodic Structures

A. One Slot in Each Cell

First, the rectangular waveguide periodic structure with one slot in each cell is analyzed. In Fig. 2, the black dotted lines represent the normalized phase and attenuation constants of the $n = -1$ space harmonic in the structure. The results can be calculated with the equations shown in Section II-C, by taking the antenna unit cell with two identical slots, a period $2p$, and a distance p between the slots. Alternatively, the results can also be calculated from the equations given in [2] for a rectangular waveguide structure with only one slot in each cell. The two results are the same, and only one result is shown with the black dotted lines in Fig. 2. Note that the equations given in [2] had been validated with simulation by HFSS and had also been validated with the measurement of an equivalent SIW structure in [21]. Hence, it confirms that the results from the equations given in Section II-C are accurate.

From the black dotted lines in Fig. 2, a very large open stopband (from 14.28 to 16.42 GHz) is observed. In the stopband, the phase constant β_{-1} remains almost zero (not exactly in this open structure), and the attenuation constant has a large bump. The large attenuation constant is mainly due to the reactive behavior in the stopband [9]. Due to the large attenuation constant in the stopband, the beamwidth becomes wide. Moreover, due to the reactive behavior in the stopband, the Bloch impedance will not be real but becomes more imaginary like [9]. Therefore, the impedance match will

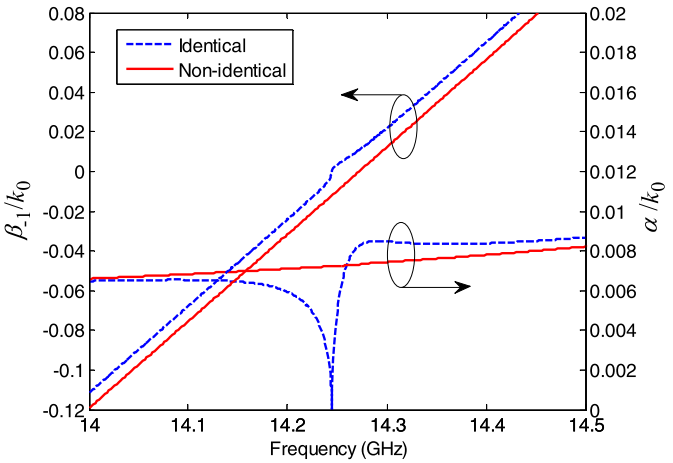

Fig. 3. Theoretical results for the normalized phase and attenuation constants for the rectangular waveguide periodic structures with two slots in each cell. One result is for the structure with two identical slots $W_1 = W_2$, the other is for the structure with two nonidentical slots of $W_1 = 0.5$ mm and $W_2 = 0.4535$ mm. The other parameters for the two structures are given in the second column in Table I.

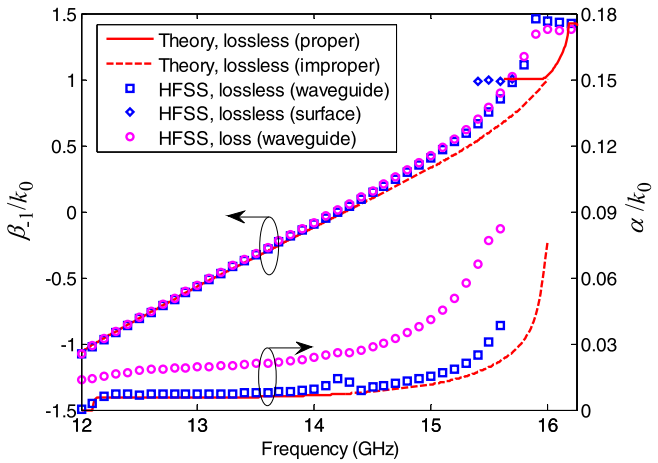

Fig. 4. Normalized phase and attenuation constants for the rectangular waveguide and the SIW periodic structures. The parameters for the rectangular waveguide structure are given in the second column in Table I. The parameters for the SIW structure are given in the second column in Table II. The simulation results from HFSS for the SIW with lossless materials are shown with square and diamond markers. The simulation results from HFSS for the SIW with lossy materials (in which the loss tangent of the substrate is $\tan\delta = 0.0023$, and the conductivity of the conductors is $\sigma = 5.8 \times 10^7$ S/m) are shown with circle markers.

become difficult and the realized gain (that accounts for the reflection coefficient) will drop drastically in the stopband [9]. A more complete discussion of the behaviors of an open stopband can be found in [9].

B. Two Identical Slots in Each Cell

Second, two identical slots are adopted for each unit cell. When the two slots are spaced by a quarter period ($d = p/4$), the open stopband can be mitigated in a certain degree. The blue dashed lines in Fig. 2 represent the normalized phase and attenuation constants of the periodic structure with two identical slots spaced by a quarter period in each cell. It is seen that its open stopband is still significant, though it is narrowed compared with the periodic structure with only one slot in each cell.

With an optimization of the distance between the two slots, the open stopband can be further mitigated. The dashed lines in Fig. 3 show the phase and attenuation constants of the structure with an optimized distance ($d = 1.0875$ mm), in an enlarged scale. It is seen that the open stopband is suppressed greatly, in which no significant large bump in the normalized attenuation constant is observed. Nevertheless, the open stopband has not yet been suppressed completely. In Fig. 3 (blue dashed lines), it is seen that the attenuation constant has a null at 14.244797 GHz, at which the normalized phase constant is not linearly with the frequency.

C. Two Nonidentical Slots Per Cell

In order to suppress the open stopband completely, two nonidentical slots are adopted for each cell. In Fig. 2, the red solid lines represent the normalized phase and attenuation constants of the periodic structure with two nonidentical slots in each cell, with the optimized parameters given in the second column in Table I. A plot with enlarged scale is shown in Fig. 3. It is seen that with two nonidentical slots for the antenna unit cell, the open stopband is completely suppressed, since the normalized phase constant (β_{-1}/k_0) of the radiation space harmonic is linearly with the frequency and the normalized attenuation constant is almost flat around broadside (where $\beta_{-1} = 0$). In this case, the normalized attenuation constant does not have a null any more at broadside.

TABLE I
OPTIMIZED PARAMETERS FOR THE RECTANGULAR WAVEGUIDE PERIODIC STRUCTURES [FIG. 1(C)]

Symbol	Fig.2-Fig.6	Fig.5-Fig.6				
L (mm)	3.5	1.5	2	2.5	3	4
d (mm)	1.0875	1.5677	1.5071	1.4123	1.2743	0.8508
W_2 (mm)	0.4535	0.4970	0.4928	0.4855	0.4735	0.417
W_1 (mm)	0.5					
a (mm)	6					
h (mm)	0.8					
ε_r	10.2					
p (mm)	6.5					
$\tan\delta$	0					
σ	∞					

In order to validate the results shown above that are calculated with the integral equation method described in Section II-C, the relating SIW periodic structure is simulated with HFSS. The propagation wavenumbers are obtained by fitting the near fields inside the SIW with exponential functions [21]. The simulation results from HFSS are shown in Fig. 4. The optimized parameters of the SIW are given in the second column in Table II. Since the method used in HFSS is very different from the theoretical method described in Section II-C, the optimized parameters from HFSS for suppressing the open stopband in the SIW are slightly different from those obtained from the theoretical method for the rectangular waveguide. Nevertheless, the two sets of optimized parameters are very close.

Fig. 4 shows that the wavenumber from HFSS for the SIW leaky-wave structure with lossless materials ($\tan\delta = 0$,

$\sigma = \infty$) is very close to the wavenumber from the theoretical calculation for the rectangular waveguide leaky-wave structure with lossless materials. When the SIW is constructed on lossy materials ($\tan\delta = 0.0023$ and $\sigma = 5.8 \times 10^7$ S/m), the attenuation constant is increased compared with that of no material loss, leading to a decrease in the radiation efficiency (as will be discussed in Section IV-D). The phase constant of the SIW with lossy materials, on the other hand, is almost the same as that with lossless materials.

In the calculation using the integral equation method in Section II-C, solutions can be found for improper and proper modes. An improper mode is related to a wave that is increased exponentially in the transverse direction, with the positive value for the imaginary part of $k_{\rho n}$ in (17) (for the radiating space harmonic). The proper mode, on the other hand, is related to a wave that is attenuated exponentially in the transverse direction, with the negative value for the imaginary part of $k_{\rho n}$ in (17). The solid lines in Fig. 4 represent proper modes, in which all the space harmonics are proper. The dashed lines in Fig. 4 represent an improper mode, in which the $n = -1$ space harmonic is improper and the others are proper. In the band from 12.1 to 14.27 GHz, the structure supports a backward leaky waveguide mode, which is proper. In the band from 14.27 to 16.01 GHz, the structure supports a forward leaky waveguide mode, which is improper. At the same time, when the main beam of the forward leaky waveguide mode is scanned to endfire (where the normalized phase constant goes to 1), the structure also supports a proper surface-wave mode (in which the normalized phase constant is slightly larger than 1). The surface-wave mode has most of its power stored at the surface of the structure, whereas the (proper or improper) waveguide modes have most of the power stored inside the waveguide. As the frequency increases, the proper surface-wave mode is involved into a proper waveguide mode. More detailed descriptions of the properties of these modes can be found in [2].

The waveguide modes and surface-wave mode can also be found from HFSS, by measuring the fields interior and exterior of the structure [2]. The results from HFSS are shown in Fig. 4 for the structure with lossless material. From Fig. 4, it is seen that the results from HFSS are consistent with those theoretically calculated by the integral equation method. (The surface-wave mode solution from HFSS for the SIW structure with lossy materials is not shown in Fig. 4.) Note that in this structure, the excitation of the surface-wave mode is rather small, so it is difficult to find the surface-wave mode in the experiment (in Section IV-C). The excitation of the surface-wave mode depends mainly on the slot size [2]. With a larger slot size, it is easier for the surface-wave mode to be excited [2], [21].

D. Optimization Procedure for the Structure With Two Nonidentical Elements

In the optimization for the complete suppression of the open stopband in a periodic structure using the proposed technique, we can start with two identical elements spaced by a quarter of the period. The optimized parameters for the complete suppression of the open stopband in the periodic rectangular leaky-wave structures with different slot lengths are given in Table I. The normalized phase and attenuation constants are shown in Figs. 5 and 6. Figs. 5 and 6 show that the open stopbands are completely suppressed. From the optimized parameters given in Table I, it is found that the width of the second slot is closer to that of the first slot and the distance between the two slots is closer to a quarter of the period, when the perturbation due to the slots is smaller (i.e., the length of the two slots is smaller, and the attenuation constant is also smaller). Hence, the optimization for the width of the second slot and the distance between the two slots can start with the width of the first slot and a quarter of the period. With a larger perturbation of the elements, the discrepancy between the final optimized parameters and the starting ones (i.e., the parameters of the first element and a quarter of the period) becomes larger.

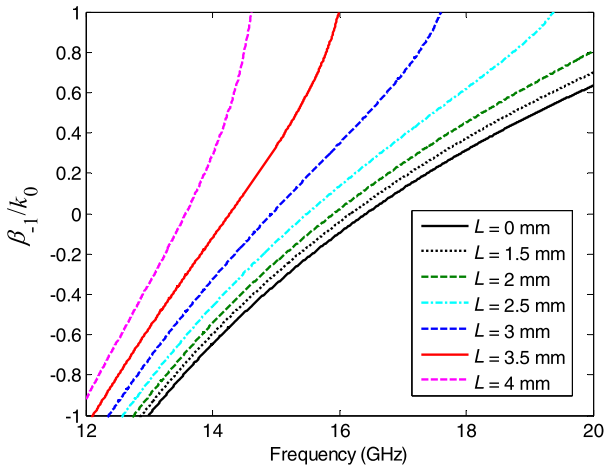

Fig. 5. Normalized phase constants for the rectangular waveguide periodic structures. The parameters are given in Table I.

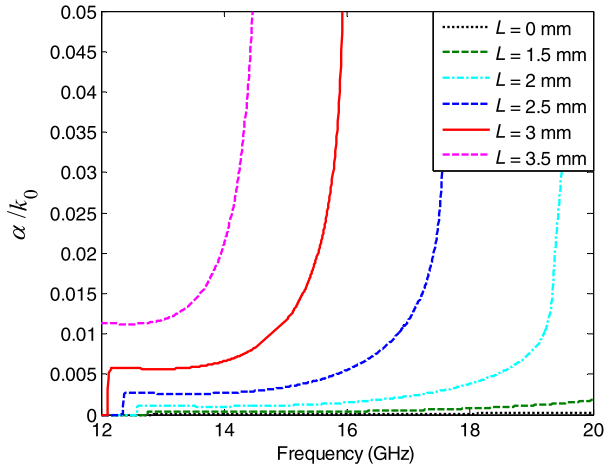

Fig. 6. Normalized attenuation constants for the rectangular waveguide periodic structures. The parameters are given in Table I.

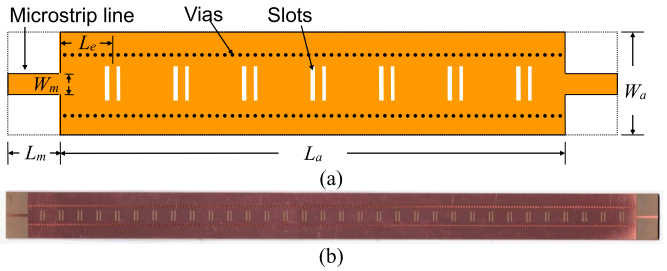

Fig. 7. (a) Geometry and (b) photograph of the designed SIW leaky-wave antenna. The geometry is not to scale. The detailed geometry of the SIW structure is given in Fig. 1(a). The parameters are given in the second column in Table II.

IV. Experiment for the SIW Periodic Antenna

A. Geometry of the Designed Antenna

A leaky-wave antenna based on the SIW periodic structure with the open stopband suppressed is designed and fabricated. The geometry and photograph of the antenna are shown in Fig. 7(a) and (b). The antenna includes 32 cells for the periodic structure. The antenna is fed by a microstrip line with a characteristic impedance of 50 Ω and terminated by a 50-Ω load. The substrate of the antenna has a relative permittivity $\varepsilon_r = 10.2$, a height $h = 1$ mm, and a tangent loss $\tan\delta = 0.0023$. The conductor in the antenna is cop, which has a conductivity $\sigma = 5.8\times10^7$ S/m. The detailed dimensions for the SIW structure are given in the second column in Table II.

B. S-Parameters

Fig. 8 shows the reflection (S_{11}) and transmission (S_{21}) coefficients for the designed antenna. Simulation result of S_{11} from HFSS shows a nearly perfect impedance matching for the antenna around broadside (around 14.2 GHz). Measured result of S_{11} is consistent with the simulation result although a frequency shift of about 0.15 GHz is observed compared with the simulation result, and the measured reflection coefficient is relatively higher than the simulation one due to fabrication error. Nevertheless, the measured result shows that the reflection coefficient is lower than −11.3 dB around broadside. In the band from 12.1 to 16 GHz where the antenna has the main beam scanned from the backward to the forward direction, the measured transmission coefficient is lower than −10 dB, meaning that less than 10% of the power is left at the loading termination.

C. Radiation Properties

Fig. 9 shows the realized gain (that accounts for the reflection coefficient) for the designed antenna. Simulation result shows that the gain keeps almost stable around broadside (around 14.2 GHz). Measured result for the gain is almost consistent with the simulation one although a discrepancy within 2 dB can be observed due to fabrication and measurement errors. The measured result shows that the antenna has a gain of about 13 dBi.

Fig. 10 shows the main beam direction [measured from the normal direction, i.e., the y-axis in Fig. 1(a)] of the antenna.

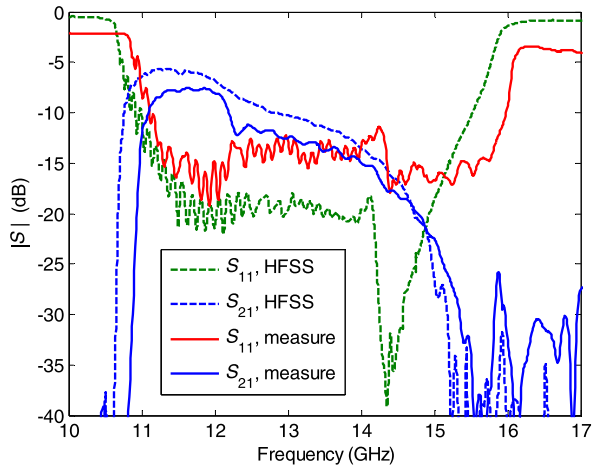

Fig. 8. Reflection and transmission coefficients for the antenna in Fig. 7.

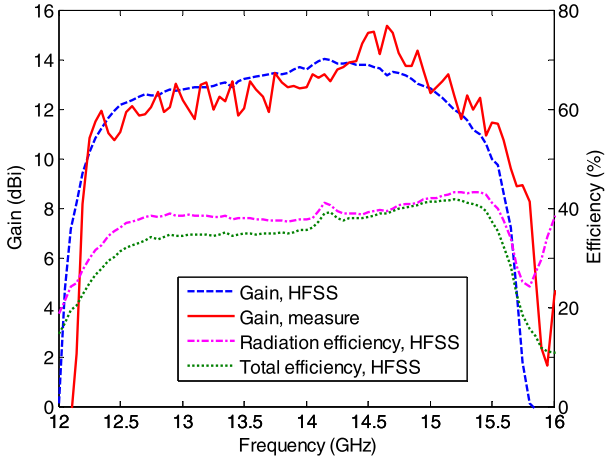

Fig. 9. Realized gain and efficiencies for the antenna in Fig. 7.

The simulation and measured results are consistent with the theoretical result [calculated by (1) where the phase constant is obtained with the integral equation method described in Section II-C (the phase constant is also shown in Fig. 2)]. Around broadside, the radiation angle behaves linearly with the frequency. With an increase of the frequency, the main beam is scanned from the backward endfire to the forward direction.

Fig. 11 shows the realized gain patterns for the antenna working at various frequencies. Since a frequency shift exits for the simulation and measured results, the frequencies for the simulated patterns are 0.15 GHz lower than those shown in Fig. 11 for the measured patterns. It is seen that the measured result is almost consistent with the simulation one. With an increase of the frequency from 12.25 to 15.6 GHz, the measured result shows that the beam is scanned from −78° to 46.5° (with the gain varying from 10.7 to 13.86 dBi).

Fig. 12(a) shows the normalized patterns for the antenna radiating at backward endfire. Simulation result shows that the antenna can have its beam at exactly endfire when it is placed on an infinite ground plane. When the antenna is placed on a finite ground plane, the main beam is titled a certain degree

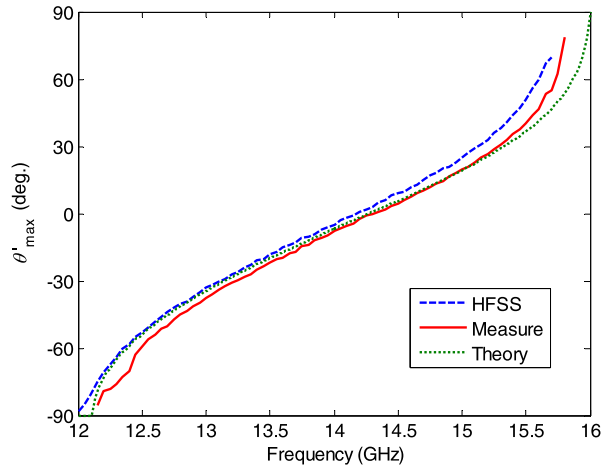

Fig. 10. Radiation angle for the antenna in Fig. 7.

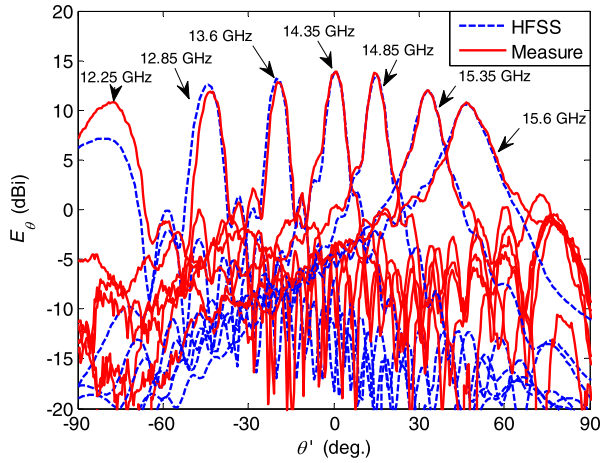

Fig. 11. Gain patterns of the co-polarized field for the antenna (Fig. 7) in the principal plane. The measured frequencies are the ones shown in this figure, whereas the simulated frequencies are 0.15 GHz lower than those values.

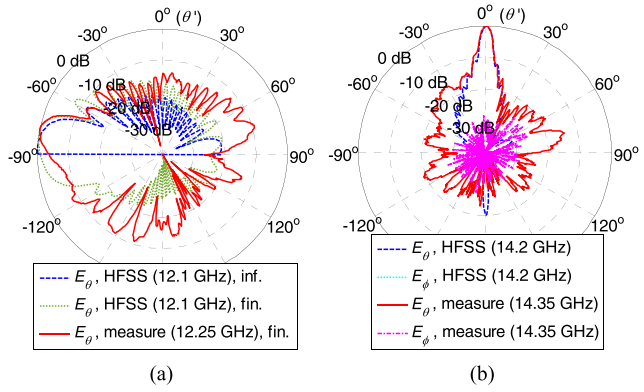

(a) (b)

Fig. 12. Normalized radiation patterns for the antenna in Fig. 7. (a) Radiation patterns at backward endfire. (b) Radiation patterns at broadside (with finite ground plane).

from the endfire direction, due to finite ground diffraction. Measured result is close to the simulation one for the case with finite ground plane.

Fig. 12(b) shows the normalized patterns for the antenna radiating at broadside. Due to a frequency shift between the simulation and measured results, the measured main beam is scanned to the broadside direction at 14.35 GHz, whereas the simulated main beam is scanned to the broadside direction at 14.2 GHz. Nevertheless, the measured and simulated patterns are in good consistence except for the frequency shift. Since most of the radiated power is from the narrow slots, the cross polarization level is very low. The simulated cross polarization level is lower than -40 dB, so that the simulated field E_ϕ cannot be observed in Fig. 12. The measured cross-polarized field E_ϕ is also very low, with a cross polarization level lower than -25 dB.

When the main beam is scanned close to forward endfire, the attenuation constant becomes high (as can be found from Fig. 4) and the radiation becomes degraded. Fig. 9 shows that the realized gain starts to drop significantly when the (measurement) frequency is over 15.6 GHz. Therefore, it is difficult for the designed antenna to have a forward endfire beam with high gain.

D. Efficiencies

The simulated radiation efficiency η_r and total efficiency η_t are shown in Fig. 9. The total efficiency is calculated by $\eta_t = (1 - |S_{11}^2| - |S_{21}^2|)\eta_r$, which accounts for the reflection loss at the excitation port and the load loss at the termination port. Since the reflection and transmission coefficients are very small (as shown in Fig. 8), the radiation efficiency is the dominant role. Fig. 12 shows that the total efficiency is about 35%–42%, due to the low radiation efficiency of only about 37%–43%. The low radiation efficiency is due to the low ratio of the leakage constant (the attenuation constant due to only leakage) to the total attenuation constant that accounts for leakage and material loss [21], as can be found from Fig. 4. The low radiation efficiency is a disadvantage of this antenna with such a high permittivity. An increase of the slot size can have a limited increase in the efficiency (about 3%). A further increase in the efficiency for the antenna with a high permittivity relies on the materials of lower loss (a lower tangent loss for the substrate and a higher conductivity for the conductors).

If a substrate of low permittivity is used, the efficiency can be increased greatly. Two SIW leaky-wave antennas with low permittivities of $\varepsilon_r = 4.5$ and $\varepsilon_r = 2.2$ are simulated using HFSS, with the parameters given in the third and fourth columns in Table II. (The tangent loss and the conductivity are assumed the same as those for the antenna with $\varepsilon_r = 10.2$.) These simulated SIW structures are of 32 cells, and are excited and terminated with 50-Ω microstrip lines. The total efficiencies for the SIW leaky-wave antennas with the low permittivities of $\varepsilon_r = 4.5$ and $\varepsilon_r = 2.2$ are shown in Fig. 13, and compare with that for the antenna with $\varepsilon_r = 10.2$. Fig. 13 shows that the efficiency can be significantly improved if the antenna employs a low permittivity. When the antenna employs a low permittivity of $\varepsilon_r = 2.2$, the total efficiency can be increased close to 70%. On the other hand, the scanning range is narrowed if a low permittivity is employed. The simulated scanning ranges $\theta'_{\max}$ for the antennas within 3-dB gain variation are given in Table II. It is seen that the scanning range for the antenna with $\varepsilon_r = 2.2$ is only from $\theta' = -48°$ to $\theta' = 13°$ for the gain variation within 3 dB.

TABLE II
PARAMETERS FOR THE SIW PERIODIC STRUCTURES [FIG. 1(A)]

Symbol	Fig. 4(a), Fig. 7-Fig. 13	Fig. 4(a), Fig. 7(a), Fig. 13	
ε_r	10.2	4.5	2.2
w	6.46 mm	9.41 mm	12.42 mm
r	0.3 mm	0.3 mm	0.3 mm
s	$p/7$	$p/10$	$p/11$
h	1 mm	1 mm	1 mm
p	6.5 mm	9 mm	12 mm
L	3.5 mm	5 mmm	6.5 mm
W_1	0.5 mm	0.7 mm	0.7 mm
W_2	0.46 mm	0.6 mm	0.53 mm
d	1.11 mm	1.34 mm	1.61 mm
L_a	212.2 mm	294.4 mm	394 mm
W_a	16 mm	20 mm	20 mm
L_e	5.36 mm	7.7 mm	11 mm
L_m	7.5 mm	10 mm	10 mm
W_m	0.93 mm	1.9 mm	3 mm
$\tan\delta$	0.0023	0.0023	0.0023
σ	5.8×10^7 S/m	5.8×10^7 S/m	5.8×10^7 S/m
$\theta'_{\max}$ (3 dB)	$-64° \sim 44°$	$-56° \sim 23°$	$-48° \sim 13°$

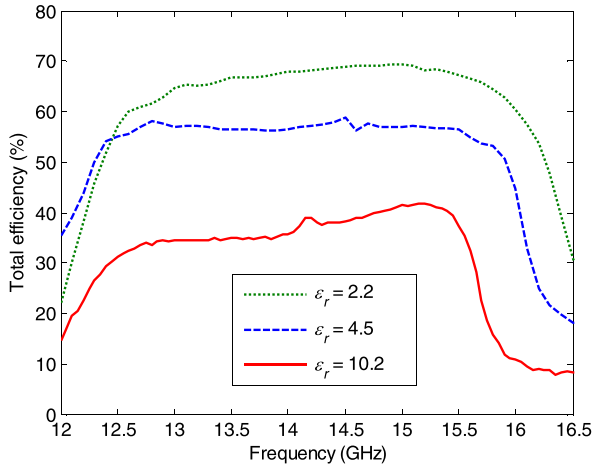

Fig. 13. Total efficiencies for the SIW periodic leaky-wave antennas of 32 cells with different permittivities. The geometry for the main SIW leaky-wave structures is shown in Fig. 1(a), and the geometry for the antenna designs is shown in Fig. 7(a). The dimensions are given in Table II.

Therefore, the antenna has a wide scanning range, but is with the dependence on a high permittivity and with a compromise in the efficiency. Compared with the SIW leaky-wave antenna with longitudinal slots [26], the presented antenna has a wider scanning range and does not suffer from blind point at backward endfire. Compared with the single-layer spoof-plasmon-mode leaky-wave antenna [29], the presented antenna has a higher gain due to that the structure has a ground plane.

V. PRINTED COMBLINE PERIODIC LEAKY-WAVE ANTENNA WITH TWO STUBS PER UNIT CELL

The proposed technique can also be applied to other periodic leaky-wave structure, e.g., a printed combline leaky-wave antenna with the unit cell [9] shown in Fig. 14(a). When the unit cell contains only one open-ended stub, as shown in Fig. 14(a), an open stopband occurs. The dashed and dotted lines in Fig. 15 represent the normalized phase and attenuation

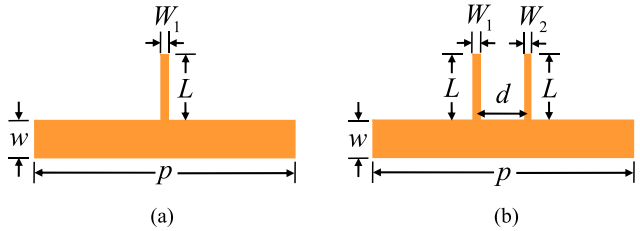

Fig. 14. Geometries for the unit cell in the combline periodic leaky-wave structures. (a) Unit cell contains one open-ended stub [9]. (b) Unit cell contains two similar but nonidentical open-ended stubs.

TABLE III
PARAMETERS FOR THE COMBLINE PERIODIC STRUCTURES

Symbol	One stub [9] (Fig.14(a), Fig.15)	Two stubs (Fig.14(b), Fig.15)
w	0.6 mm	0.6 mm
ε_r	10.2	10.2
h	0.676 mm	0.676 mm
p	4 mm	4 mm
L	0.5 mm	0.5 mm
W_1	0.1 mm	0.1 mm
W_2		0.076 mm
d		1.01 mm
$\tan\delta$	0	0
σ	∞	∞

constants for the structure. It is seen that the open stopband simulated from HFSS is very close to that calculated from the integral method in [9]. A small discrepancy between the two results is observed (especially for the phase constant), due to that the two numerical methods (in HFSS and in [9]) are very different. Nevertheless, the two results are very close around broadside. Moreover, a deep minimum for the attenuation constant is observed in both results at broadside frequency.

If the unit cell of the combline structure contains two similar but slightly different open-ended stubs, as shown in Fig. 14(b), the open stopband can be eliminated. The solid lines in Fig. 15 show the normalized phase and attenuation constants for the combline periodic structure with two nonidentical stubs. It is seen that the open stopband is completely suppressed, since its normalized attenuation constant behaves flat against the frequency around broadside. The optimized parameters for the structure with the open stopband suppressed are given in Table III.

The design procedure for the open-stopband suppressed structure is very simple. To design the structure with the open stopband suppressed, we need only to optimize the distance d between the two stubs and the length W_2 of the second stub (assuming that the two stubs share the same length). In the optimization for d and W_2, we can start with a quarter of the period ($p/4$) and the width of the first stub (W_1). From Table III, we see that the optimized distance $d = 1.01$ mm and the width $W_2 = 0.076$ mm are very close to a quarter of the period $p/4 = 1$ mm and the width of the first stub $W_1 = 0.1$ mm. Of course, a stopband-suppressed structure with two stubs of different lengths (but of identical width) can also be designed. (It is also possible to have a similar stopband-suppressed design of the structure using the procedure in [12].

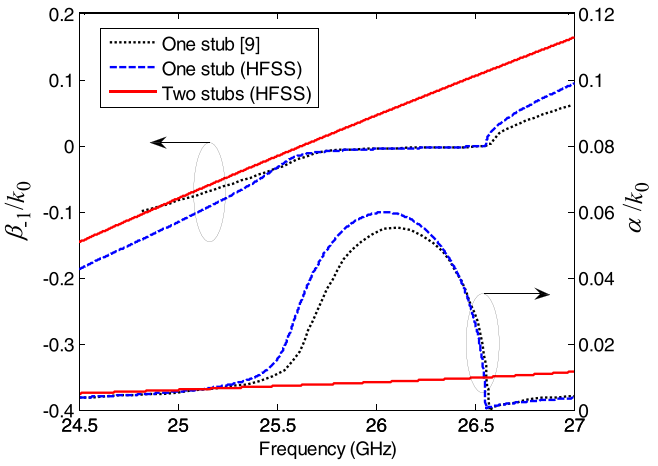

Fig. 15. Normalized phase and attenuation constants for the combline leaky-wave structures. The structures are given in Fig. 14, and the parameters are given in Table III.

However, the design procedure in [12] is far more complicated than the presented one.)

In this case of the open stopband suppression, the shunt element (open-ended stub) is far from the resonant length (half wavelength). Therefore, the series resonance is far from the shunt resonance if the unit cell contains only one stub. Nevertheless, the technique can effectively suppress the open stopband, without frequency balancing the series and shunt resonances as in [12].

VI. Conclusion

A simple technique has been proposed for the complete suppression of the open stopband in periodic leaky-wave antennas using two similar but nonidentical elements for each unit cell. In the design procedure, one needs only to optimize the distance between the two elements and the dimension of the second element, starting with a quarter of the period and the dimension of the first element.

Two periodic leaky-wave antennas with the open stopband suppressed using the technique have been demonstrated. An SIW periodic leaky-wave antenna with two transverse slots per unit cell is developed and investigated. Simulation and measured results are consistent with the theoretical results. The antenna has a high gain and a wide scanning range from the backward endfire to the forward direction. Besides the SIW antenna, a combline periodic leaky-wave antenna is demonstrated, in which the open stopband is suppressed using two similar but nonidentical open-ended stubs per unit cell. The two antennas validate the effectiveness of the technique. The technique is simple, and is expected to be applied to various periodic leaky-wave antennas based on different structures, e.g., waveguide, dielectric image line, SIW, and microstrip line.

Acknowledgment

The authors would like to thank the reviewers for their useful suggestions that have helped to improve this paper.

References

[1] R. Hyneman, "Closely-spaced transverse slots in rectangular waveguide," *IRE Trans. Antennas Propag.*, vol. 7, no. 4, pp. 335–342, Oct. 1959.

[2] J. Liu, D. R. Jackson, and Y. Long, "Modal analysis of dielectric-filled rectangular waveguide with transverse slots," *IEEE Trans. Antennas Propag.*, vol. 59, no. 9, pp. 3194–3203, Sep. 2011.

[3] J. Liu and Y. Long, "A full-wave numerical approach for analyzing rectangular waveguides with periodic slots," *IEEE Trans. Antennas Propag.*, vol. 60, no. 8, pp. 3754–3762, Aug. 2012.

[4] K. Solbach and B. Adelseck, "Dielectric image line leaky wave antenna for broadside radiation," *Electron. Lett.*, vol. 19, no. 16, pp. 640–641, Aug. 1983.

[5] J. R. James and P. S. Hall, "Microstrip antennas and arrays. Part 2: New array-design technique," *IEE J. Microw., Opt. Antennas*, vol. 1, no. 5, pp. 175–181, Sep. 1977.

[6] J. R. James, P. Hall, and C. Wood, *Microstrip Antenna Theory and Design*. London, U.K.: Peter Peregrinus Ltd., 1981.

[7] M. Guglielmi and D. R. Jackson, "Broadside radiation from periodic leaky-wave antennas," *IEEE Trans. Antennas Propag.*, vol. 41, no. 1, pp. 31–37, Jan. 1993.

[8] C. Caloz and T. Itoh, *Electromagnetic Metamaterials: Transmission Line Theory and Microwave Applications*. New York, NY, USA: Wiley, 2005.

[9] S. Paulotto, P. Baccarelli, F. Frezza, and D. R. Jackson, "A novel technique for open-stopband suppression in 1-D periodic printed leaky-wave antennas," *IEEE Trans. Antennas Propag.*, vol. 57, no. 7, pp. 1894–1906, Jul. 2009.

[10] J. T. Williams, P. Baccarelli, S. Paulotto, and D. R. Jackson, "1-D combline leaky-wave antenna with the open-stopband suppressed: Design considerations and comparisons with measurements," *IEEE Trans. Antennas Propag.*, vol. 61, no. 9, pp. 4484–4492, Sep. 2013.

[11] S. Otto, A. Al-Bassam, A. Rennings, K. Solbach, and C. Caloz, "Radiation efficiency of longitudinally symmetric and asymmetric periodic leaky-wave antennas," *IEEE Antennas Wireless Propag. Lett.*, vol. 11, pp. 612–615, 2012.

[12] S. Otto, A. Al-Bassam, A. Rennings, K. Solbach, and C. Caloz, "Transversal asymmetry in periodic leaky-wave antennas for Bloch impedance and radiation efficiency equalization through broadside," *IEEE Trans. Antennas Propag.*, vol. 62, no. 10, pp. 5037–5054, Oct. 2014.

[13] S. Otto, Z. Chen, A. Al-Bassam, A. Rennings, K. Solbach, and C. Caloz, "Circular polarization of periodic leaky-wave antennas with axial asymmetry: Theoretical proof and experimental demonstration," *IEEE Trans. Antennas Propag.*, vol. 62, no. 4, pp. 1817–1829, Apr. 2014.

[14] A. Al-Bassam, S. Otto, D. Heberling, and C. Caloz, "Broadside dual-channel orthogonal-polarization radiation using a double-asymmetric periodic leaky-wave antenna," *IEEE Trans. Antennas Propag.*, vol. 65, no. 6, pp. 2855–2864, Jun. 2017.

[15] M. H. Rahmani and D. Deslandes, "Backward to forward scanning periodic leaky-wave antenna with wide scanning range," *IEEE Trans. Antennas Propag.*, vol. 65, no. 7, pp. 3326–3335, Jul. 2017.

[16] D. Deslandes and K. Wu, "Substrate integrated waveguide leaky-wave antenna: Concept and design considerations," in *Proc. Asia–Pacific Microw. Conf.*, Dec. 2005, pp. 346–349.

[17] F. Xu, K. Wu, and X. Zhang, "Periodic leaky-wave antenna for millimeter wave applications based on substrate integrated waveguide," *IEEE Trans. Antennas Propag.*, vol. 58, no. 2, pp. 340–347, Feb. 2010.

[18] Y. J. Cheng, W. Hong, and K. Wu, "Millimeter-wave half mode substrate integrated waveguide frequency scanning antenna with quadri-polarization," *IEEE Trans. Antennas Propag.*, vol. 58, no. 6, pp. 1848–1855, Jun. 2010.

[19] Y. J. Cheng, W. Hong, K. Wu, and Y. Fan, "Millimeter-wave substrate integrated waveguide long slot leaky-wave antennas and two-dimensional multibeam applications," *IEEE Trans. Antennas Propag.*, vol. 59, no. 1, pp. 40–47, Jan. 2011.

[20] Y. D. Dong and T. Itoh, "Composite right/left-handed substrate integrated waveguide and half mode substrate integrated waveguide leaky-wave structures," *IEEE Trans. Antennas Propag.*, vol. 59, no. 3, pp. 767–775, Mar. 2011.

[21] J. Liu, D. R. Jackson, and Y. Long, "Substrate integrated waveguide (SIW) leaky-wave antenna with transverse slots," *IEEE Trans. Antennas Propag.*, vol. 60, no. 1, pp. 20–29, Jan. 2012.

[22] J. Liu, X. Tang, Y. Li, and Y. Long, "Substrate integrated waveguide leaky-wave antenna with H-shaped slots," *IEEE Trans. Antennas Propag.*, vol. 60, no. 8, pp. 3962–3967, Aug. 2012.

[23] A. J. Martinez-Ros, J. L. Gómez-Tornero, and G. Goussetis, "Holographic pattern synthesis with modulated substrate integrated waveguide line-source leaky-wave antennas," *IEEE Trans. Antennas Propag.*, vol. 61, no. 7, pp. 3466–3474, Jul. 2013.
[24] J. Machac, M. Polivka, and K. Zemlyakov, "A dual band leaky wave antenna on a CRLH substrate integrated waveguide," *IEEE Trans. Antennas Propag.*, vol. 61, no. 7, pp. 3876–3879, Jul. 2013.
[25] J. Liu, D. R. Jackson, Y. Li, C. Zhang, and Y. Long, "Investigations of SIW leaky-wave antenna for endfire-radiation with narrow beam and sidelobe suppression," *IEEE Trans. Antennas Propag.*, vol. 62, no. 9, pp. 4489–4497, Sep. 2014.
[26] A. Mallahzadeh and S. Mohammad-Ali-Nezhad, "Periodic collinear-slotted leaky wave antenna with open stopband elimination," *IEEE Trans. Antennas Propag.*, vol. 63, no. 12, pp. 5512–5521, Dec. 2015.
[27] Z. Li, J. Wang, M. Chen, and Z. Zhang, "New approach of radiation pattern control for leaky-wave antennas based on the effective radiation sections," *IEEE Trans. Antennas Propag.*, vol. 63, no. 7, pp. 2867–2878, Jul. 2015.
[28] Y. Geng, J. Wang, Y. Li, Z. Li, M. Chen, and Z. Zhang, "Leaky-wave antenna array with a power-recycling feeding network for radiation efficiency improvement," *IEEE Trans. Antennas Propag.*, vol. 65, no. 5, pp. 2689–2694, May 2017.
[29] A. Kianinejad, Z. N. Chen, and C.-W. Qiu, "A single-layered spoof-plasmon-mode leaky wave antenna with consistent gain," *IEEE Trans. Antennas Propag.*, vol. 65, no. 2, pp. 681–687, Feb. 2017.
[30] D. R. Jackson and A. A. Oliner, "Leaky-wave antennas," in *Modern Antenna Handbook*, C. A. Balanis, Ed. Hoboken, NJ, USA: Wiley, 2008, ch. 7.
[31] L. Yan, W. Hong, K. Wu, and T. J. Cui, "Investigations on the propagation characteristics of the substrate integrated waveguide based on the method of lines," *IEE Proc.-Microw., Antennas Propag.*, vol. 152, no. 1, pp. 35–42, Feb. 2005.

Juhua Liu (M'12) was born in Heyuan, Guangdong, China, in 1981. He received the B.S. and Ph.D. degrees in electrical engineering from Sun Yat-sen University, Guangzhou, China, in 2004 and 2011, respectively.

From 2008 to 2009, he was a Visiting Scholar with the Department of Electrical and Computer Engineering, University of Houston, Houston, TX, USA. From 2011 to 2012, he was a Senior Research Associate with the State Key Laboratory of Millimeter Waves, City University of Hong Kong, Hong Kong. From 2012 to 2015, he was a Lecturer with the Department of Electronics and Communication Engineering, Sun Yat-sen University, where he has been an Associate Professor since 2015. His current research interests include microstrip antennas, substrate-integrated waveguide antennas, leaky-wave antennas, periodic structures, and computational electromagnetics.

Wenlong Zhou was born in Dongguan, Guangdong, China, in 1993. He received the B.S. degree in electrical engineering from Sun Yat-sen University, Guangzhou, China, in 2016, where he is currently pursuing the M.Eng. degree.

His current research interests include microstrip antennas, substrate-integrated waveguide antennas, circularly polarized antennas, and leaky-wave antennas.

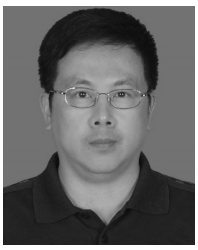

Yunliang Long (M'01–SM'02) was born in Chongqing, China, in 1963. He received the B.Sc., M.Eng., and Ph.D. degrees from the University of Electronic Science and Technology of China, Chengdu, China, in 1983, 1989, and 1992, respectively.

From 1992 to 1994, he was a Post-Doctoral Research Fellow and an Associate Professor with the Department of Electronics, Sun Yat-sen University, Guangzhou, China, where he is currently a Professor and the Head of the Department of Electronics and Communication Engineering. From 1998 to 1999, he was a Visiting Scholar with IHF, RWTH University of Aachen, Aachen, Germany. From 2000 to 2001, he was a Research Fellow with the Department of Electronics Engineering, City University of Hong Kong, Hong Kong. He has authored or co-authored over 130 academic papers. His current research interests include antennas and propagation theory, electromagnetic theory in inhomogeneous lossy medium, computational electromagnetics, and wireless communication applications.

Dr. Long is a member of the Committee of Microwave Society of CIE, and on the Editorial Board of the *Chinese Journal of Radio Science*. He is the Vice Chairman of the Guangzhou Electronic Industrial Association. His name is listed in *Who's Who in the World*.